

# Photolithographic Patterning of Perovskite Thin Films for Multicolor Display Applications

Chen Zou, Cheng Chang, Di Sun, Karl F. Böhringer, and Lih Y. Lin\*

Cite This: *Nano Lett.* 2020, 20, 3710–3717

Read Online

ACCESS |

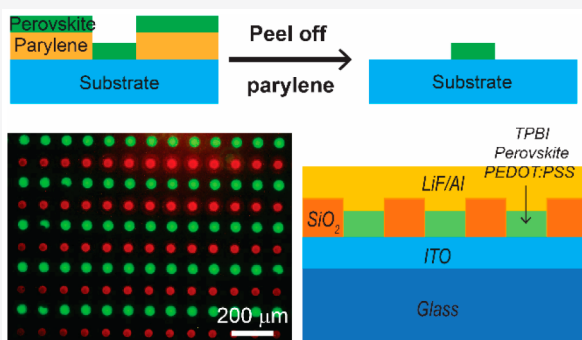
Metrics & More

Article Recommendations

Supporting Information

**ABSTRACT:** Metal halide perovskites are emerging as attractive materials for light-emitting diode (LED) applications. The external quantum efficiency (EQE) has experienced a rapid progress and reached over 21%, comparable to the state of the art organic and quantum dot LEDs. For metal halide perovskites, their simple solution-processing preparation, facile band gap tunability, and narrow emission line width provide another attractive route to harness their superior optoelectronic properties for multicolor display applications. In this work, we demonstrate a high-resolution, large-scale photolithographic method to pattern multicolor perovskite films. This approach is based on a dry lift-off process which involves the use of parylene as an intermediary and the easy mechanical peeling-off of parylene films on various substrates. Using this approach, we successfully fabricated multicolor patterns with red and green perovskite pixels on a single substrate, which could be further applied in liquid crystal displays (LCDs) with blue backlight. Besides, a prototype green perovskite micro-LED display under current driving has been demonstrated.

**KEYWORDS:** metal halide perovskite, photolithography, dry lift-off, multicolor display, micro-LED



## INTRODUCTION

In the past several decades, patterning techniques of solution-processed luminescent materials have been attracting intense interests for their broad application prospects in full-color displays, image sensors, and lasers.<sup>1–4</sup> High-resolution lithographic patterning methods such as photolithography and electron-beam lithography have been widely adopted in organic and quantum dot (QD) optoelectronics,<sup>5–7</sup> promoting the commercialized applications of organic and QD micro- and nanoscale devices including televisions (TVs), cameras, and thin-film transistor (TFT) planes.

Metal halide perovskites have recently successfully emerged as promising materials for a wide variety of applications in solar cells, light-emitting diodes (LEDs), photodetectors, and lasers.<sup>8–12</sup> They stand out from other conventional semiconductor materials not only for their excellent optoelectronic properties but also for their facile solution processability and widely tunable band gap.<sup>13</sup> Previous works on solar cells rely on narrow-band-gap iodine-based perovskites to absorb light in a wide wavelength range. The true benefit of band gap tunability is reflected in light-emitting applications, where strong and narrow line width emissions covering a broad range of wavelengths are particularly in need.

In the past several years, along with the booming development of perovskite solar cells, much effort has also been devoted to light-emitting applications of perovskite materials. The photoluminescence quantum yield (PLQY) of

perovskite materials has been improved to over 90%.<sup>14</sup> Prominent progress has also been achieved recently for perovskite LEDs (PeLEDs); the external quantum efficiency (EQE) has reached over 20% for green and red PeLEDs, and 10% for blue PeLEDs.<sup>15–19</sup> However, these studies are mainly focused on synthesis, photophysics, and device engineering. The development of patterning perovskite films, especially using lithographic methods, has been comparatively lacking and imperfect,<sup>20</sup> and lithographically patterned perovskite micro-LED arrays have not been demonstrated. This difference is likely caused by the ionic nature of perovskite materials, which makes them tend to be dissolved in common polar solvents that are often used in high-resolution lithographic methods.<sup>21</sup>

To avoid the difficulties in lithographic methods, many researchers have developed alternative methods to pattern perovskite films. Most noticeable, several groups utilized the inkjet printing technique to form polycrystalline perovskite patterns on various substrates.<sup>22–25</sup> However, inkjet printing is a low-throughput process and requires specially formulated

Received: February 17, 2020

Revised: April 17, 2020

Published: April 23, 2020



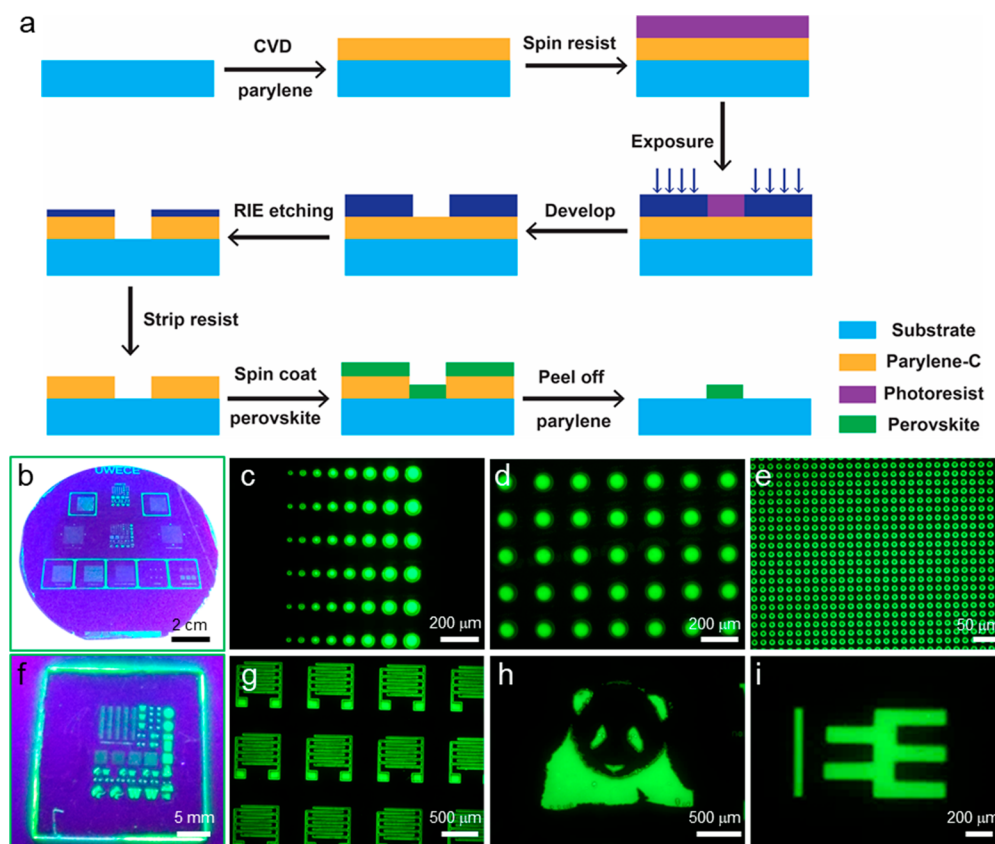


**Figure 1.** (a) Schematic fabrication procedures for high-resolution photolithographic patterning of perovskite thin films. (b, f) Optical images of green perovskite patterns on a 4 in. silicon wafer and a 1 in. glass square under excitation from a UV lamp. (c) Perovskite circles with diameters varying from 20 to 90  $\mu\text{m}$ . Uniform arrays of (d) 100  $\mu\text{m}$  and (e) 10  $\mu\text{m}$  perovskite circles (scale bar 50  $\mu\text{m}$ ). (g) Interdigitated electrode (IDE) patterns. (h) Cartoon image of a panda. (i) UW EE department logo.

inks and substrate heating. Nanoimprinting has also been applied to produce perovskite patterns. Wang et al. and Pourdavoud et al. thermally embossed grating and photonic crystal structures to perovskite films.<sup>26,27</sup> Several other groups used the imprinted PDMS template to force perovskite solutions to crystallize into desired structures.<sup>28–31</sup> However, these methods could deteriorate the optoelectronic properties of perovskites and affect device performance.

In industry, the preferable fabrication method for commercialized products such as multicolor displays and image sensors is photolithography, as it provides good pattern quality with high resolutions, high throughput, great reproducibility, and wafer-scale manufacturing. Recently, Wu et al. and Kim et al. photolithographically patterned a self-assembled (SAM) layer to form alternative hydrophobic and hydrophilic areas.<sup>3,32</sup> The perovskite precursor was spin-coated onto the SAM layer, and patterns were formed based on wetting and dewetting properties of the surface. Lin et al. photolithographically patterned fluorinated polymer (orthogonal resist) and exploited an orthogonal solvent to lift-off perovskite films.<sup>33</sup> The orthogonal resist and solvent need to be chosen carefully to ensure that the solvent dissolves the resist but not the perovskite. Harwell et al. used double-layer resists on top of perovskite layers in a photolithographic process and finally etched perovskites with argon milling.<sup>34</sup> However, this method involves complicated procedures and physically etching perovskites.

In this work, we report a generic approach to pattern perovskites photolithographically in micrometer resolution

based on a dry lift-off process. No solvent is needed in this lift-off process, thus avoiding the dissolution problem of perovskite in common polar solvents. The excellent optoelectronic properties of perovskite materials are preserved throughout the fabrication process. Based on this approach, red, green, and blue (RGB) single-color perovskite patterns are successfully fabricated. In addition, we also demonstrate multicolor perovskite patterns with green and red emissions simultaneously on one substrate, which could be further applied in liquid crystal display (LCD) applications. The blue backlight could be absorbed and converted to green and red color light, enabling full-color displays. Finally, perovskite micro-LED displays based on this novel patterning method have been achieved for the first time, to the best of our knowledge. The devices show a maximum EQE of 1.24%, current efficiency of 3.85 cd/A, and luminance of 13 043 cd/m<sup>2</sup>. Our work demonstrates the great potential of perovskites for multicolor displays and paves the way for commercialization of perovskite micro- and nanoscale devices.

## RESULTS AND DISCUSSION

**1. Single-Color Patterns.** For photolithographic patterning of perovskite thin films, the lift-off process may be preferable as it avoids the process of etching perovskites. However, the problem with this process still exists in finding appropriate orthogonal solvents and resists to address the incompatibility of perovskites with the solvents used for photoresist removal. Here, we developed a dry lift-off process which relies on the limited adhesion of parylene to various

substrates.<sup>35,36</sup> The type of parylene we used in this work is parylene-C as it has a very low permeability to solvents. Figure 1a depicts the fabrication procedures of patterning perovskite thin films. First, a  $\sim 2.5$   $\mu\text{m}$  thick parylene film was deposited onto the clean substrate by room-temperature chemical vapor deposition (CVD). Subsequently, standard photolithography was used to fabricate desired trenches in the photoresist layer (step 3–5). The patterned trenches were then transferred to the parylene film by reactive ion etching (RIE). The remaining photoresist was stripped by  $\text{O}_2$  plasma or acetone. Then, the perovskite precursor was spin-coated to the substrate followed by annealing at 100  $^\circ\text{C}$  to promote the crystallization. To increase the PLQY of perovskite thin films, we used quasi-2D perovskites here due to their better exciton confinement provided by the multiple quantum wells structure.<sup>37</sup> For green perovskite precursors, approximate amounts of phenethylammonium bromide (PEABr), CsBr, and  $\text{PbBr}_2$  were mixed in dimethyl sulfoxide (DMSO) solvent. The PLQY of green perovskite films could reach over 70% (Figure S1 in the Supporting Information). For blue and red perovskites, part of the bromide halides was replaced by chloride and iodine halides, respectively. Finally, the underlying parylene film was easily peeled off by a narrow-tip tweezer (Figure S2). Using this approach, we could pattern large-scale and multicolor perovskite films on various substrates.

Figure 1b,f shows the optical images of perovskite patterns on a 4 in. silicon wafer and 1 in. glass substrates under ultraviolet (UV) lamp excitation. Figure 1c–e presents fluorescent images of perovskite circles with different diameters. Circles of 10  $\mu\text{m}$  were successfully achieved as shown in Figure 1e. Examples of an interdigitated electrode pattern, a cartoon image of a panda, and the UW EE department logo are presented in Figure 1g–i. All these images show strong green luminescence with high color contrast, demonstrating the successful application of this dry lift-off process for patterning perovskites. Furthermore, using this protocol, we are able to achieve a high patterning resolution for perovskite films. The micropatterning of features as small as 4  $\mu\text{m}$  is possible (Figure S3). Although the demonstrations above were done using quasi-2D perovskites, our approach can be extended to other types of metal halide perovskites such as perovskite quantum dots (QDs)<sup>8</sup> and vacuum-deposited perovskites<sup>38</sup> (Figures S4 and S5). We also examined the surface morphologies by atomic force microscopy (AFM) and PL profiles of patterns made from quasi-2D, QD, and vacuum-deposited perovskites (Figure S6). The quasi-2D perovskite circles were found to possess a nestlike topography, where elevated rims are formed toward the circumference. Consequently, the PL intensity from the center is 60% of that from the edge. These results are consistent with the work reported by Lin et al.<sup>33</sup> The nonuniform topography is a common issue for spin-coating processes and depends on many parameters such as choice of solvent, solution viscosity, spin-speed, and dispense approach (static and dynamic dispense). It is interesting to note that perovskite QD circles show more uniform height and PL profiles compared to quasi-2D perovskites, which may be due to the different solvent used for these two perovskite solutions (hexane for perovskite QDs and DMSO for quasi-2D perovskites). To avoid the nonuniform topography from spin-coating processes, thermal evaporation was adopted to vacuum-deposited perovskite films. As a result, perovskite patterns from vacuum-deposition show uniform height and PL profiles. However, among these

perovskite materials, quasi-2D perovskites are widely used in high-performance LED applications due to their high PLQY, good charge transport, and simple preparation method.<sup>37,39,40</sup> We will use quasi-2D perovskite films in the following work unless otherwise specified.

Other color perovskite patterns have also been demonstrated in this work. The optical images of RGB-emission perovskite films under UV excitation show strong PL for all these colors (Figure S7). Blue, green, and red perovskite circles (50  $\mu\text{m}$  diameter) are shown in Figure 2a–c. RGB 10  $\mu\text{m}$

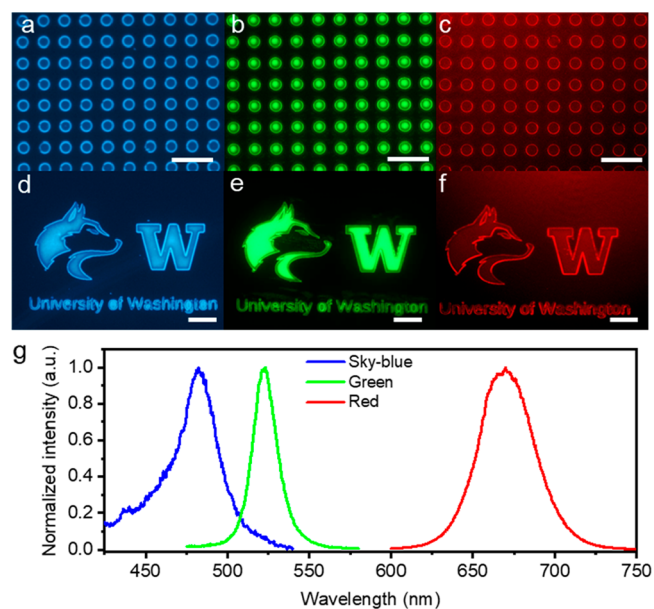


**Figure 2.** (a–c) Blue, green, and red perovskite circles (50  $\mu\text{m}$  diameter). (d–f) University of Washington logos, scale bar 200  $\mu\text{m}$ . (g) PL spectra of blue, green, and red perovskite films.

circles were also successfully fabricated (Figure S8), corresponding to a high resolution of 1270 dots per inch (dpi). In addition, the University of Washington logos emitting blue, green, and red light are displayed in Figure 2d–f. Blue and green perovskite patterns show strong luminescence with high color contrast while red ones suffer from relatively low contrast due to the environmental instability of red perovskites. Figure 2g shows blue, green, and red perovskite emission spectra. The peak wavelength is 482, 523, and 670 nm for blue-, green-, and red-emission perovskite thin films, respectively. The green perovskite films show the narrowest line width of  $\sim 17$  nm while the line width is  $\sim 28$  and  $\sim 38$  nm for blue and red perovskite films, respectively.

**2. Multicolor Patterns.** For commercial RGB displays, one solution is to fabricate green and red pixels together on one substrate with a blue backlight underneath; this is widely used in LCD applications.<sup>2,7</sup> The green- and red-emission pixels could absorb blue light and convert it to green and red light, thus achieving real RGB displays. Herein, we use standard photolithography with the demonstrated dry lift-off process twice to pattern green and red perovskite sequentially on a glass substrate. Figure 3a schematically illustrates the fabrication procedures. The parylene and photoresist were sequentially deposited onto the substrate with prefabricated green perovskite patterns. The standard photolithography and RIE were used again to generate patterned trenches in the parylene film. The red perovskite precursor was spin-cast and

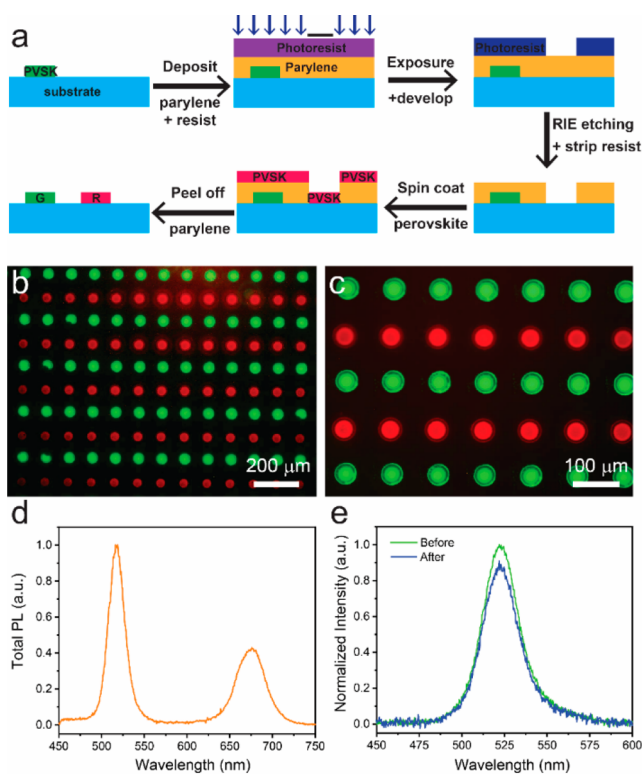


**Figure 3.** (a) Schematic fabrication procedures of multicolor perovskite patterns. (b) Fluorescent microscope image of green and red perovskite circles with a diameter of  $50 \mu\text{m}$ . (c) Higher-magnification fluorescent image of the dual-color patterns. (d) Overall PL spectrum of the dual-color perovskite patterns. (e) PL spectra comparison of green perovskite patterns before and after the second patterning process.

annealed for a short time. After peeling off the parylene film, multicolor perovskite patterns were successfully formed. Figure 3b displays the uniform array of alternative green and red perovskite circles; each circle has a diameter of  $\sim 50 \mu\text{m}$ . The magnified fluorescent image is shown in Figure 3c; the second photolithography and lift-off processes did not affect the prefabricated green perovskite patterns due to the excellent sealing of parylene films. The perovskite films covered by parylene could even survive in acetone solution for several days. We also measured the overall PL spectrum contributed by both green and red perovskite circles at the same time (Figure 3d). The overall PL from multicolor patterns shows two emission peaks located separately at green and red wavelength regions. The peak PL intensity of green perovskite patterns is about 2.5-fold as high as that of red ones. This difference can be easily understood considering the relatively poor PLQY and stability of red-emission perovskites which include more iodine halides. Figure 3e shows the PL spectra of green perovskite patterns before and after the second patterning process. No peak wavelength shift is observed, and only a slight drop of PL intensity is seen after going through the second patterning process. To further verify that our approach is effective and nonintrusive, we measured the absolute PLQY evolution of green perovskite films during multicolor patterning processes (Figure S9). The PLQY remains essentially the same after the first patterning process and only slightly drops from  $69 \pm 7\%$  to  $62 \pm 8\%$  after the second patterning process. This is likely due to the degradation

of perovskite patterns caused by long-time exposure to environment moisture and resist baking in the second photolithography process. These results indicate that our approach preserves the properties of prefabricated perovskite patterns properly, and thus, multiple patterning processes are feasible.

**3. Perovskite Micro-LED Displays.** Another solution for achieving RGB displays is to develop self-emissive arrays of RGB pixels under the current-driving mode.<sup>1,2</sup> The emission of the display is controlled by the current flowing to individual pixels through a TFT back plane. Nowadays, this solution has been widely adopted in commercial LED TVs. Through the proposed photolithographic method with dry lift-off, we successfully demonstrated a green pixelated perovskite micro-LED array for the first time, to the best of our knowledge. Figure 4a schematically depicts the structure of PeLEDs with green pixels. To avoid the current shunt path between the cathode and anode, an insulating layer ( $\text{SiO}_2$ ) was deposited and etched to separate PeLED pixels. The functional layers including poly(3,4-ethylenedioxythiophene) polystyrenesulfonate (PEDOT:PSS), perovskite, and 2,2',2''-(1,3,5-benzene-triyl)-tris(1-phenyl-1-*H*-benzimidazole) (TPBi) were patterned based on the above-mentioned photolithographic method. Finally, the top electrode was deposited to finish fabrication. The energy level diagram of PeLEDs is shown in Figure 4b; the electrons and holes are injected from indium tin oxide (ITO) and aluminum (Al), respectively, and recombine in the perovskite layer to emit photons. Figure 4c–e displays various current-driving PeLED patterns including an array of  $20 \mu\text{m}$  diameter circles, an array of  $30 \mu\text{m}$  square patterns, and a University of Washington logo. These images were obtained by an optical microscope in dark field (Figure S10). Uniform electroluminescence (EL) from PeLED pixels was observed. Figure 4f shows the EL spectra of pixelated PeLEDs at various biases from 3 to 5 V. The EL spectra exhibit a narrow line width of 19 nm, indicating a high color purity of PeLEDs which is of importance in display applications. The inset photo in Figure 4f shows a green-emission PeLED with many squared subpixels operated at a bias of 4 V. The device exhibits great emission homogeneity without any obvious dead pixels, just like a single unit. Pixelated PeLEDs with blue and red emission can be fabricated in a similar approach based on our proposed method.

The performance of the pixelated PeLEDs ( $30 \mu\text{m}$  square array with 100 pixels) was further characterized. Figure 5a shows the luminance ( $L$ )–current density ( $J$ )–voltage ( $V$ ) characteristics. The current density and luminance were calculated based on the total area of PeLED pixels. It is clearly observed that the devices show typical diode characteristics; the current density increases exponentially with voltage. The turn on voltage of the devices is determined to be about 3.4 V (defined as the voltage at which a luminance of  $1 \text{ cd}/\text{m}^2$  is obtained). The maximum luminance of  $13\,043 \text{ cd}/\text{m}^2$  is achieved at 8.4 V, and the luminance starts to decrease after that because of Joule heat and Auger recombination. The dependence of EQE and current efficiency on current density is shown in Figure 5b. The device exhibits a maximum EQE of 1.24%, current efficiency of  $3.85 \text{ cd}/\text{A}$ , and luminous efficiency of  $1.86 \text{ lm}/\text{W}$ . However, in comparison, reference PeLEDs (nonpatterned) show a peak EQE of 3.9% (Figure S11). To analyze this difference, we compared the performance of devices that went through various processing steps in Figures S12 and S13. We attribute the deteriorated performance of

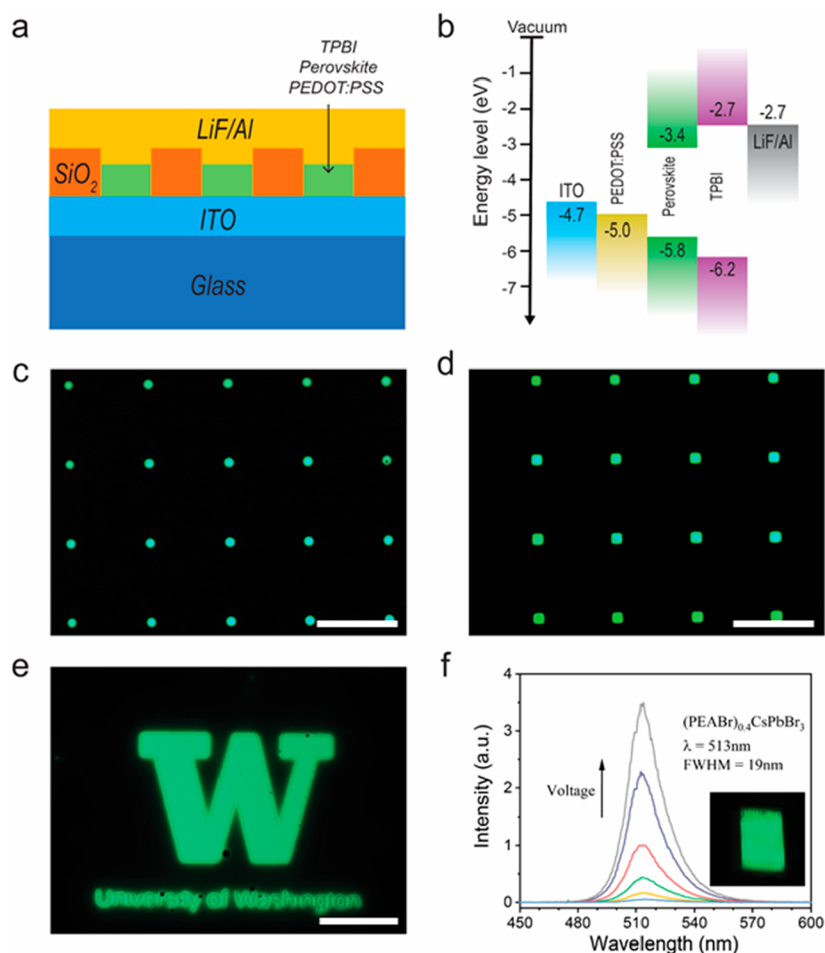


**Figure 4.** (a) Schematic structure of pixelated PeLEDs. (b) Energy level diagram. (c–e) Optical microscope images (in dark field) of electrically driven perovskite patterns; the scale bar is  $200\ \mu\text{m}$ : (c)  $20\ \mu\text{m}$  diameter circles, (d)  $30\ \mu\text{m}$  squares, and (e) University of Washington logo. (f) EL spectra of pixelated PeLEDs at various voltages from 3 to 5 V. The inset photograph shows a large emitting area ( $2 \times 2\ \text{mm}^2$ ) with patterned perovskite squares.

pixelated PeLEDs to the larger leakage current compared to that of reference devices, which is likely due to a few existing bad pixels in a large array and imperfect pixel edges after the dry lift-off process. Further device optimization should be focused on improving the surface uniformity of patterned perovskite pixels to minimize the leakage current.

## CONCLUSION

In summary, we have succeeded in developing a high-resolution, large-area photolithographic method to pattern perovskite thin films using parylene as an intermediary. The utilization of parylene enables a dry lift-off process where unwanted perovskite is mechanically lifted off without the aid of orthogonal solvents. Based on this approach, RGB single-color patterns have been successfully fabricated. Thus far, the highest pattern resolution we can achieve is down to  $4\ \mu\text{m}$ . The parylene films are also able to protect the perovskite films underneath well, enabling multicolor perovskite patterns by using the standard photolithography process multiple times. Finally, an electrically driven green perovskite display consisting of a perovskite micro-LED array has been demonstrated with high color purity and contrast. The pixelated PeLEDs show a peak EQE of 1.24% and maximum luminance of  $13\ 043\ \text{cd}/\text{m}^2$ . We have also demonstrated that our photolithographic patterning approach is generic and can

be applied to various types of metal halide perovskites including quasi-2D perovskites, perovskite quantum dots,<sup>8</sup> and vacuum-deposited perovskites.<sup>38</sup> Our work demonstrates the feasibility of patterning multicolor perovskite thin films and supports the promising potentials of perovskites for commercialized multicolor displays.

## EXPERIMENTAL SECTION

**Materials.**  $\text{PbCl}_2$ ,  $\text{PbBr}_2$ ,  $\text{PbI}_2$ ,  $\text{CsBr}$ ,  $\text{CsI}$ , PEABr, and dimethyl sulfoxide (DMSO, anhydrous) were purchased from Sigma-Aldrich. PEDOT:PSS (AI 4083) and TPBi (>98% purity) were purchased from Ossila. 1,4,7,10,13,16-Hexaoxacyclooctadecane (18-crown-6, crown) (99% purity) was purchased from Acros. Aluminum pellets were purchased from Kurt J. Lesker.

**Preparation of Perovskite Films.** The green perovskite precursor was obtained by mixing 0.2 M  $\text{CsBr}$ , 0.2 M  $\text{PbBr}_2$ , 0.08 M PEABr, and crown in DMSO. The blue perovskite precursor was obtained by mixing 0.2 M  $\text{CsBr}$ , 0.1 M  $\text{PbBr}_2$ , 0.1 M  $\text{PbCl}_2$ , 0.16 M PEABr, and crown in DMSO. The red perovskite precursor was obtained by mixing 0.2 M  $\text{CsI}$ , 0.2 M  $\text{PbI}_2$ , 0.08 M PEABr, and crown in DMSO. The addition of crown is to improve the surface morphology and PLQY of perovskite films as reported elsewhere.<sup>41</sup> Unless specified, the concentration of crown is  $3.5\ \text{mg}/\text{mL}$  in perovskite solutions.

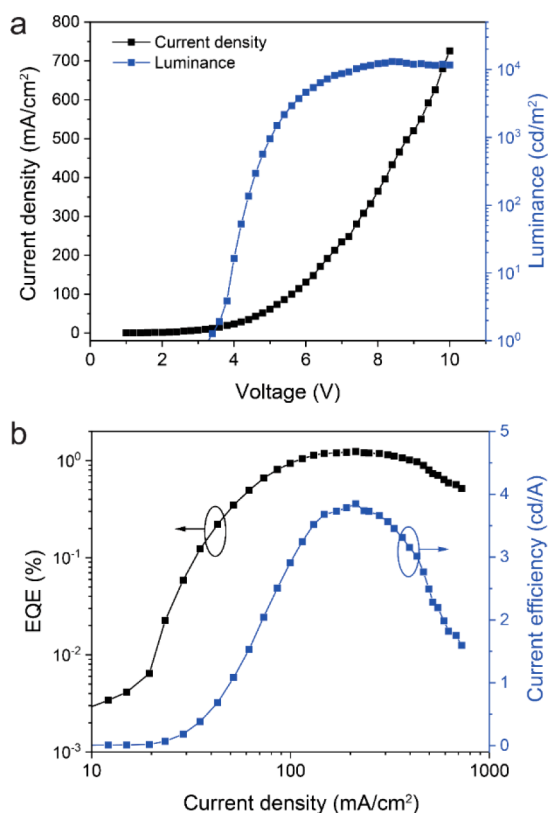


**Figure 5.** Performance characterization of pixelated PeLEDs. (a)  $L$ – $J$ – $V$  characteristics. (b) Plot of EQE and current efficiency versus current density.

All precursors were heated at 60 °C for 2 h with constant stirring. The perovskite precursors were spin-coated onto substrates at 3000 rpm for 60 s with an acceleration speed of 1500 rpm/s. Afterward, the perovskite films were immediately annealed at 100 °C for 1 min to accelerate nucleation.

**Fabrication of Patterned Perovskite Films.** For single-color patterns, the parylene-C film was deposited onto a substrate at room temperature by a CVD process (PDS 2010, SCS Labcoater 2). 5 g of parylene-C powders was placed inside the furnace. The furnace, vaporizer, and vacuum set points are 690 °C, 175 °C, and 35 mTorr, respectively. The deposition chamber was kept at room temperature. The thickness of the parylene film was measured to be around 2.5  $\mu\text{m}$  by a stylus profilometer (DektakXT, Bruker). The negative photoresist NR9-3000 was spin-coated onto the parylene film with a two-step process (1000 rpm for 5 s and 3000 rpm for 45 s) and then prebaked at 110 °C for 5 min. The photoresist was then exposed to 365 nm UV light ( $\sim 9 \text{ mW}/\text{cm}^2$ ) for 20 s (ABM semiauto-aligner) and baked at 100 °C for 5 min. The photoresist was developed in AD10 solution for 30 s and cleaned in deionized (DI) water for 15 s. The patterns should be clearly seen at this stage. The parylene film was then etched by an RIE process with mixed  $\text{SF}_6$  (5 sccm) and  $\text{O}_2$  (50 sccm) gas. The RF power was set as 250 W, and the process pressure was 40 mTorr. The etch rate was measured as 350 nm per minute, and the parylene film was etched for 9.5 min. The selectivity of the photoresist to parylene was 1.2:1, so the photoresist was usually etched away after the RIE process. However, acetone or  $\text{O}_2$  plasma could be used to strip the remaining photoresist. The RGB perovskite precursors were then spin-cast using the above-mentioned method. The

parylene film was mechanically peeled off by a narrow-tip tweezer with desired perovskite patterns remaining on the substrate. Multiple standard photolithography processes could be used sequentially to pattern multicolor perovskite films on a single substrate.

**Characterization of Perovskite Films.** The PL spectra of perovskite films and patterns were measured by our homemade micro-PL system. A continuous wave (CW) laser ( $\lambda = 405 \text{ nm}$ ) was used as the excitation source, and the laser beam was focused onto the sample through an objective lens. The location of the laser beam was observed by a CCD camera (Chameleon 3, FLIR). The PL emission was collected by a pair of convex lenses and focused onto an optical spectrometer (OSM 100, Newport). The surface morphologies of perovskite patterns were analyzed by AFM (ICON, Bruker). The fluorescent images of perovskite patterns were obtained by a fluorescent microscope (EVOS, Thermo Fisher Scientific).

**Fabrication of Micro-LED Displays.** To avoid the electrical shunt path between ITO and Al, a 120 nm thick  $\text{SiO}_2$  layer was deposited by plasma enhanced chemical vapor deposition (PECVD) at 125 °C onto ITO-coated glass substrates. The parylene film was deposited onto  $\text{SiO}_2$  by CVD at room temperature. The parylene film was then etched using the same above-mentioned procedure. The trenches were transferred to the  $\text{SiO}_2$  layer by RIE with a gas mixture of  $\text{CF}_4$  and  $\text{CHF}_3$ . PEDOT:PSS was spin-coated at 4000 rpm and annealed at 110 °C for 10 min; the annealing temperature should not be over 130 °C as parylene may become softened at this temperature and hard to peel off afterward. The green perovskite precursor was spin-cast as above-mentioned. The samples were then transferred into a thermal evaporator, and the chamber was pumped to a base pressure below  $2 \times 10^{-6}$  Torr. TPBi (40 nm) and LiF (1 nm) were thermally evaporated at a rate of 0.8 and 0.3  $\text{\AA}/\text{s}$ , respectively. Finally, functional layers were lifted off by peeling off the parylene film. The top electrode Al (70 nm) was deposited through thermal evaporation at a rate of 2  $\text{\AA}/\text{s}$ . The  $\text{SiO}_2$  layer works as a separator layer to isolate individual micro-LED pixels.

**Characterization of Perovskite Micro-LEDs.** The current density–voltage ( $J$ – $V$ ) characteristics were measured by a source meter (Keithley 6430). Simultaneously, front-face EL power output from the ITO side was measured by a calibrated silicon photodiode (Newport 818-SL). The EQE was calculated as the ratio of the number of emitted photons to the number of injected electrons. The EL spectra of PeLEDs were measured by a fiber-coupled spectrometer (OSM 100, Newport). All device measurements were carried out under ambient conditions. The EL images of perovskite micro-LED displays were obtained by an optical microscope in dark field.

## ■ ASSOCIATED CONTENT

### Supporting Information

The Supporting Information is available free of charge at <https://pubs.acs.org/doi/10.1021/acs.nanolett.0c00701>.

Additional experimental methods; PLQY measurements; optical images of various perovskite patterns; patterning resolution of our approach; fluorescent images of perovskite QD and vacuum-deposited perovskite patterns; topography characterization of perovskite patterns; fluorescent images of RGB quasi-2D perovskite thin films and 10  $\mu\text{m}$  circles; experimental setup for recording EL from pixelated PeLEDs; and performance

comparison between pixelated PeLEDs and non-patterned reference devices (PDF)

## AUTHOR INFORMATION

### Corresponding Author

Lih Y. Lin – Department of Electrical and Computer Engineering, University of Washington, Seattle, Washington 98195, United States; [orcid.org/0000-0001-9748-5478](https://orcid.org/0000-0001-9748-5478); Email: [lylin@uw.edu](mailto:lylin@uw.edu)

### Authors

Chen Zou – Department of Electrical and Computer Engineering, University of Washington, Seattle, Washington 98195, United States; [orcid.org/0000-0001-9638-6363](https://orcid.org/0000-0001-9638-6363)

Cheng Chang – Department of Electrical and Computer Engineering, University of Washington, Seattle, Washington 98195, United States

Di Sun – Department of Electrical and Computer Engineering, University of Washington, Seattle, Washington 98195, United States

Karl F. Böhringer – Department of Electrical and Computer Engineering, University of Washington, Seattle, Washington 98195, United States; [orcid.org/0000-0002-9428-2648](https://orcid.org/0000-0002-9428-2648)

Complete contact information is available at:

<https://pubs.acs.org/10.1021/acs.nanolett.0c00701>

### Author Contributions

C.Z. and L.Y.L. conceived the project. C.Z. carried out all the experiments and data analysis. L.Y.L. supervised the project. C.C. contributed to the photomask fabrication. D.S. and K.F.B. contributed to the discussion and technical support on parylene patterning. C.Z. drafted the manuscript, and all authors provided inputs to the manuscript revision and agreed to the final version.

### Notes

The authors declare no competing financial interest.

## ACKNOWLEDGMENTS

This work is supported by the National Science Foundation (Grant ECCS-1807397) and IP group LLC. Part of the work was conducted at the Washington Nanofabrication Facility, a National Nanotechnology Coordinated Infrastructure site at the University of Washington supported by the National Science Foundation (Grant NNCI-1542101).

## REFERENCES

(1) Kim, T.-H.; Cho, K.-S.; Lee, E. K.; Lee, S. J.; Chae, J.; Kim, J. W.; Kim, D. H.; Kwon, J.-Y.; Amaratunga, G.; Lee, S. Y.; Choi, B. L.; Kuk, Y.; Kim, J. M.; Kim, K. Full-Colour Quantum Dot Displays Fabricated by Transfer Printing. *Nat. Photonics* **2011**, *5*, 176–182.

(2) Dai, X.; Deng, Y.; Peng, X.; Jin, Y. Quantum-Dot Light-Emitting Diodes for Large-Area Displays: Towards the Dawn of Commercialization. *Adv. Mater.* **2017**, *29*, 1607022.

(3) Wu, W.; Wang, X.; Han, X.; Yang, Z.; Gao, G.; Zhang, Y.; Hu, J.; Tan, Y.; Pan, A.; Pan, C. Flexible Photodetector Arrays Based on Patterned  $\text{CH}_3\text{NH}_3\text{PbI}_{3-x}\text{Cl}_x$  Perovskite Film for Real-Time Photosensing and Imaging. *Adv. Mater.* **2019**, *31*, 1805913.

(4) Prins, F.; Kim, D. K.; Cui, J.; De Leo, E.; Spiegel, L. L.; McPeak, K. M.; Norris, D. J. Direct Patterning of Colloidal Quantum-Dot Thin Films for Enhanced and Spectrally Selective Out-Coupling of Emission. *Nano Lett.* **2017**, *17*, 1319–1325.

(5) Lee, E. K.; Park, C. H.; Lee, J.; Lee, H. R.; Yang, C.; Oh, J. H. Chemically Robust Ambipolar Organic Transistor Array Directly Patterned by Photolithography. *Adv. Mater.* **2017**, *29*, 1605282.

(6) Park, J.-S.; Kyhm, J.; Kim, H. H.; Jeong, S.; Kang, J.; Lee, S.-e.; Lee, K.-T.; Park, K.; Barange, N.; Han, J. Alternative Patterning Process for Realization of Large-Area, Full-Color, Active Quantum Dot Display. *Nano Lett.* **2016**, *16*, 6946–6953.

(7) Lin, S.; Tan, G.; Yu, J.; Chen, E.; Weng, Y.; Zhou, X.; Xu, S.; Ye, Y.; Yan, Q. F.; Guo, T. Multi-Primary-Color Quantum-Dot Down-Converting Films for Display Applications. *Opt. Express* **2019**, *27*, 28480–28493.

(8) Swarnkar, A.; Marshall, A. R.; Sanehira, E. M.; Chernomordik, B. D.; Moore, D. T.; Christians, J. A.; Chakrabarti, T.; Luther, J. M. Quantum Dot-Induced Phase Stabilization of (-CsPbI<sub>3</sub> Perovskite for High-Efficiency Photovoltaics. *Science* **2016**, *354*, 92–95.

(9) Zhao, B.; Bai, S.; Kim, V.; Lamboll, R.; Shivanna, R.; Auras, F.; Richter, J. M.; Yang, L.; Dai, L.; Alsari, M.; She, X.-J.; Liang, L.; Zhang, J.; Lilliu, S.; Gao, P.; Snaith, H. J.; Wang, J.; Greenham, N. C.; Friend, R. H.; Di, D. High-Efficiency Perovskite-Polymer Bulk Heterostructure Light-Emitting Diodes. *Nat. Photonics* **2018**, *12*, 783–789.

(10) Lin, Q.; Armin, A.; Burn, P. L.; Meredith, P. Filterless Narrowband Visible Photodetectors. *Nat. Photonics* **2015**, *9*, 687–694.

(11) Jia, Y.; Kerner, R. A.; Grede, A. J.; Rand, B. P.; Giebink, N. C. Continuous-Wave Lasing in an Organic-Inorganic Lead Halide Perovskite Semiconductor. *Nat. Photonics* **2017**, *11*, 784–788.

(12) Huang, C.-Y.; Zou, C.; Mao, C.; Corp, K. L.; Yao, Y.-C.; Lee, Y.-J.; Schlenker, C. W.; Jen, A. K. Y.; Lin, L. Y. CsPbBr<sub>3</sub> Perovskite Quantum Dot Vertical Cavity Lasers with Low Threshold and High Stability. *ACS Photonics* **2017**, *4*, 2281–2289.

(13) Kim, Y. H.; Cho, H.; Heo, J. H.; Kim, T. S.; Myoung, N.; Lee, C. L.; Im, S. H.; Lee, T. W. Multicolored Organic/Inorganic Hybrid Perovskite Light-Emitting Diodes. *Adv. Mater.* **2015**, *27*, 1248–1254.

(14) Braly, I. L.; deQuilettes, D. W.; Pazos-Outón, L. M.; Burke, S.; Ziffer, M. E.; Ginger, D. S.; Hillhouse, H. W. Hybrid Perovskite Films Approaching the Radiative Limit with over 90% Photoluminescence Quantum Efficiency. *Nat. Photonics* **2018**, *12*, 355–361.

(15) Lin, K.; Xing, J.; Quan, L. N.; de Arquer, F. P. G.; Gong, X.; Lu, J.; Xie, L.; Zhao, W.; Zhang, D.; Yan, C.; Li, W.; Liu, X.; Lu, Y.; Kirman, J.; Sargent, E. H.; Xiong, Q.; Wei, Z. Perovskite Light-Emitting Diodes with External Quantum Efficiency Exceeding 20 Per Cent. *Nature* **2018**, *562*, 245–248.

(16) Wang, Q.; Wang, X.; Yang, Z.; Zhou, N.; Deng, Y.; Zhao, J.; Xiao, X.; Rudd, P.; Moran, A.; Yan, Y.; Huang, J. Efficient Sky-Blue Perovskite Light-Emitting Diodes via Photoluminescence Enhancement. *Nat. Commun.* **2019**, *10*, 5633.

(17) Cao, Y.; Wang, N.; Tian, H.; Guo, J.; Wei, Y.; Chen, H.; Miao, Y.; Zou, W.; Pan, K.; He, Y.; Cao, H.; Ke, Y.; Xu, M.; Wang, Y.; Yang, M.; Du, K.; Fu, Z.; Kong, D.; Dai, D.; Jin, Y.; et al. Perovskite Light-Emitting Diodes Based on Spontaneously Formed Submicrometre-Scale Structures. *Nature* **2018**, *562*, 249–253.

(18) Chiba, T.; Hayashi, Y.; Ebe, H.; Hoshi, K.; Sato, J.; Sato, S.; Pu, Y.-J.; Ohisa, S.; Kido, J. Anion-Exchange Red Perovskite Quantum Dots with Ammonium Iodine Salts for Highly Efficient Light-Emitting Devices. *Nat. Photonics* **2018**, *12*, 681–687.

(19) Xu, W.; Hu, Q.; Bai, S.; Bao, C.; Miao, Y.; Yuan, Z.; Borzda, T.; Barker, A. J.; Tyukalova, E.; Hu, Z. Rational Molecular Passivation for High-Performance Perovskite Light-Emitting Diodes. *Nat. Photonics* **2019**, *13*, 418–424.

(20) Yang, X.; Wu, J.; Liu, T.; Zhu, R. Patterned Perovskites for Optoelectronic Applications. *Small Methods* **2018**, *2*, 1800110.

(21) Lyashenko, D.; Perez, A.; Zakhidov, A. High-Resolution Patterning of Organohalide Lead Perovskite Pixels for Photodetectors Using Orthogonal Photolithography. *Phys. Status Solidi A* **2017**, *214*, 1600302.

(22) Liu, Y.; Li, F.; Qiu, L.; Yang, K.; Li, Q.; Zheng, X.; Hu, H.; Guo, T.; Wu, C.; Kim, T. W. Fluorescent Microarrays of in Situ Crystallized Perovskite Nanocomposites Fabricated for Patterned Applications by Using Inkjet Printing. *ACS Nano* **2019**, *13*, 2042–2049.

(23) Wong, Y. C.; Wu, W. B.; Wang, T.; Ng, J. A.; Khoo, K. H.; Wu, J.; Tan, Z. K. Color Patterning of Luminescent Perovskites via Light-

Mediated Halide Exchange with Haloalkanes. *Adv. Mater.* **2019**, *31*, 1901247.

(24) Shi, L.; Meng, L.; Jiang, F.; Ge, Y.; Li, F.; Wu, X. g.; Zhong, H. In Situ Inkjet Printing Strategy for Fabricating Perovskite Quantum Dot Patterns. *Adv. Funct. Mater.* **2019**, *29*, 1903648.

(25) Gu, Z.; Wang, K.; Li, H.; Gao, M.; Li, L.; Kuang, M.; Zhao, Y. S.; Li, M.; Song, Y. Direct-Writing Multifunctional Perovskite Single Crystal Arrays by Inkjet Printing. *Small* **2017**, *13*, 1603217.

(26) Wang, H.; Haroldson, R.; Balachandran, B.; Zakhidov, A.; Sohal, S.; Chan, J. Y.; Zakhidov, A.; Hu, W. Nanoimprinted Perovskite Nanograting Photodetector with Improved Efficiency. *ACS Nano* **2016**, *10*, 10921–10928.

(27) Pourdavoud, N.; Wang, S.; Mayer, A.; Hu, T.; Chen, Y.; Marianovich, A.; Kowalsky, W.; Heiderhoff, R.; Scheer, H. C.; Riedl, T. Photonic Nanostructures Patterned by Thermal Nanoimprint Directly into Organo-Metal Halide Perovskites. *Adv. Mater.* **2017**, *29*, 1702902.

(28) Mao, J.; Sha, W. E. I.; Zhang, H.; Ren, X.; Zhuang, J.; Roy, V. A. L.; Wong, K. S.; Choy, W. C. H. Novel Direct Nanopatterning Approach to Fabricate Periodically Nanostructured Perovskite for Optoelectronic Applications. *Adv. Funct. Mater.* **2017**, *27*, 1606525.

(29) Brittman, S.; Oener, S. Z.; Guo, K.; Āboliņš, H.; Koenderink, A. F.; Garnett, E. C. Controlling Crystallization to Imprint Nanophotonic Structures into Halide Perovskites Using Soft Lithography. *J. Mater. Chem. C* **2017**, *5*, 8301–8307.

(30) Liu, P.; He, X.; Ren, J.; Liao, Q.; Yao, J.; Fu, H. Organic-Inorganic Hybrid Perovskite Nanowire Laser Arrays. *ACS Nano* **2017**, *11*, 5766–5773.

(31) Kamminga, M. E.; Fang, H. H.; Loi, M. A.; Ten Brink, G. H.; Blake, G. R.; Palstra, T. T. M.; Ten Elshof, J. E. Micropatterned 2D Hybrid Perovskite Thin Films with Enhanced Photoluminescence Lifetimes. *ACS Appl. Mater. Interfaces* **2018**, *10*, 12878–12885.

(32) Lee, W.; Lee, J.; Yun, H.; Kim, J.; Park, J.; Choi, C.; Kim, D. C.; Seo, H.; Lee, H.; Yu, J. W.; Lee, W. B.; Kim, D. H. High-Resolution Spin-on-Patterning of Perovskite Thin Films for a Multiplexed Image Sensor Array. *Adv. Mater.* **2017**, *29*, 1702902.

(33) Lin, C. H.; Zeng, Q.; Lafalce, E.; Yu, S.; Smith, M. J.; Yoon, Y. J.; Chang, Y.; Jiang, Y.; Lin, Z.; Vardeny, Z. V.; Tsukruk, V. V. Large-Area Lasing and Multicolor Perovskite Quantum Dot Patterns. *Adv. Opt. Mater.* **2018**, *6*, 1800474.

(34) Harwell, J.; Burch, J.; Fikouras, A.; Gather, M. C.; Di Falco, A.; Samuel, I. D. W. Patterning Multicolor Hybrid Perovskite Films via Top-Down Lithography. *ACS Nano* **2019**, *13*, 3823–3829.

(35) DeFranco, J. A.; Schmidt, B. S.; Lipson, M.; Malliaras, G. G. Photolithographic Patterning of Organic Electronic Materials. *Org. Electron.* **2006**, *7*, 22–28.

(36) Sun, D.; Böhringer, K. F. EWOD-Aided Droplet Transport on Texture Ratchets. *Appl. Phys. Lett.* **2020**, *116*, 093702.

(37) Yang, X.; Zhang, X.; Deng, J.; Chu, Z.; Jiang, Q.; Meng, J.; Wang, P.; Zhang, L.; Yin, Z.; You, J. Efficient Green Light-Emitting Diodes Based on Quasi-Two-Dimensional Composition and Phase Engineered Perovskite with Surface Passivation. *Nat. Commun.* **2018**, *9*, 570.

(38) Zou, C.; Zheng, J.; Chang, C.; Majumdar, A.; Lin, L. Y. Nonvolatile Rewritable Photomemory Arrays Based on Reversible Phase-Change Perovskite for Optical Information Storage. *Adv. Opt. Mater.* **2019**, *7*, 1900558.

(39) Wang, Z.; Wang, F.; Sun, W.; Ni, R.; Hu, S.; Liu, J.; Zhang, B.; Alsaed, A.; Hayat, T.; Tan, Z. a. Manipulating the Trade-off Between Quantum Yield and Electrical Conductivity for High-Brightness Quasi-2D Perovskite Light-Emitting Diodes. *Adv. Funct. Mater.* **2018**, *28*, 1804187.

(40) Li, Z.; Chen, Z.; Yang, Y.; Xue, Q.; Yip, H. L.; Cao, Y. Modulation of Recombination Zone Position for Quasi-Two-Dimensional Blue Perovskite Light-Emitting Diodes with Efficiency Exceeding 5%. *Nat. Commun.* **2019**, *10*, 1027.

(41) Ban, M.; Zou, Y.; Rivett, J. P. H.; Yang, Y.; Thomas, T. H.; Tan, Y.; Song, T.; Gao, X.; Credgington, D.; Deschler, F.; Siringhaus, H.; Sun, B. Solution-Processed Perovskite Light Emitting Diodes with

Efficiency Exceeding 15% through Additive-Controlled Nanostructure Tailoring. *Nat. Commun.* **2018**, *9*, 3892.